

Incorporating Posterior Model Discrepancy into a Hierarchical Framework to Facilitate Out-of-the-Box MCMC Sampling for Geothermal Inverse Problems and Uncertainty Quantification

Oliver J. Maclaren¹, Ruanui Nicholson¹, Elvar K. Bjarkason¹ & Michael J. O'Sullivan¹

¹Department of Engineering Science, The University of Auckland, Auckland, New Zealand

Key Points:

- We consider geothermal inverse problems and uncertainty quantification from a Bayesian perspective
- We incorporate posterior model approximation error into a hierarchical Bayesian framework
- This makes standard out-of-the-box MCMC sampling feasible for more complex models

Corresponding author: Oliver J. Maclaren, oliver.maclaren@auckland.ac.nz

Corresponding author: Ruanui Nicholson, ruanui.nicholson@auckland.ac.nz

Abstract

We consider geothermal inverse problems and uncertainty quantification from a Bayesian perspective. Our goal is to make standard, ‘out-of-the-box’ Markov chain Monte Carlo (MCMC) sampling more feasible for complex simulation models. To do this, we first show how to pose the inverse and prediction problems in a hierarchical Bayesian framework. We then show how to incorporate so-called posterior model approximation error into this hierarchical framework, using a modified form of the Bayesian approximation error (BAE) approach. This enables the use of a ‘coarse’, approximate model in place of a finer, more expensive model, while also accounting for the additional uncertainty and potential bias that this can introduce. Our method requires only simple probability modelling and only modifies the target posterior – the same standard MCMC sampling algorithm can be used to sample the new target posterior. We show that our approach can achieve significant computational speed-ups on a geothermal test problem. A problem which would take around a year to carry out full MCMC sampling for, now only takes around a day or so using our approach. We also demonstrate the dangers of naively using coarse, approximate models in place of finer models, without accounting for model discrepancies. The naive approach tends to give overly confident and biased posteriors, while incorporating BAE into our hierarchical framework corrects for this while maintaining computational efficiency and ease-of-use.

1 Introduction

1.1 Geothermal Modelling and Inverse Problems

Computational modelling plays an important role in geothermal reservoir engineering and resource management. A significant task for decision making and prediction in geothermal resource management is so-called *inverse modelling*, which requires solving *inverse problems*. This is also known as model calibration within the geothermal community, and consists of determining parameters compatible with measured data. This is in contrast to so-called *forward modelling* in which a simulation is based on known model parameters. A comprehensive review of geothermal modelling, including both forward modelling and model calibration, is given in (O’Sullivan et al., 2001).

The primary parameters of interest in geothermal inverse problems include the anisotropic permeability of the subsurface and the location and strength of so-called deep heat sources.

For example, knowledge of the values of these parameters allows for forecasts to be made. On the other hand, the available (i.e. directly measurable) quantities are instead typically temperature, pressure and enthalpy at observation wells (O’Sullivan and O’Sullivan, 2016; O’Sullivan et al., 2001). A typical geothermal inverse problem for a natural state, pre-exploitation model then consists of, for example, estimating formation permeabilities based on measurements of the state of the reservoir at observation wells which have been drilled into the subsurface. This may be augmented with a production history simulation where matching pressure and production enthalpy data can be used to estimate local-scale permeability and porosity. Re-running the forward problem using parameter estimates obtained by solving the inverse problem is then a natural approach to solving *prediction* or *forecasting* problems based on these measurements. The model-based prediction problem thus typically first requires the solution of an inverse problem.

When solving geothermal inverse problems, the predominant method used is still manual calibration (Burnell et al., 2012; Mannington et al., 2004; O’Sullivan and O’Sullivan, 2016; O’Sullivan et al., 2009), although it is well-recognised that this is far from an optimal strategy. To address this situation, there has recently been a concerted effort to automate the calibration process. For example, software packages such as iTOUGH2 (Finsterle, 2000) and PEST (Doherty, 2015) have been developed, and used, for geothermal model calibration. These packages are primarily based on framing the inverse problem as one of finding the minimum of a regularized cost, or objective function; though essentially deterministic, if the inverse of the Hessian is also evaluated at the minimizer then this can be used to provide approximate confidence (or credibility) intervals for model parameters. Even for optimization-based approaches to geothermal inverse problems, computations can be expensive and improvements are required to speed up the process. We recently proposed accelerating optimization-based solution methods using adjoint methods and randomized linear algebra (Bjarkason et al., 2018).

1.2 Bayesian Approaches to Geothermal Inverse Problems

Bayesian inference is an alternative, inherently probabilistic framework for inverse problems (Kaipio and Somersalo, 2005; Stuart, 2010; Tarantola, 2004). This naturally allows for quantification of uncertainty in the estimated parameters: when posed in the Bayesian setting the solution to the inverse problem is an entire probability density over the parameters. In principle this is a ‘global’ approach, and doesn’t require finding, or

centering uncertainty estimates at, a particular minimizer/maximizer. For computationally intensive problems, however, it is common to restrict attention to finding the maximum a posteriori (MAP) estimate, i.e. the point which maximizes the posterior probability density, and this becomes essentially equivalent to the deterministic, optimization-based approach. Similarly, localised uncertainty quantification can be carried out by taking the Laplace approximation to the posterior, i.e. fitting a Gaussian density function centred at the MAP estimate.

There is only a small amount of literature taking a fully Bayesian approach to geothermal inverse problems (e.g. Cui et al., 2011; Maclaren et al., 2016), where by ‘fully Bayesian’ we mean sampling the full posterior rather than calculating MAP estimates and local approximations to the posterior covariance matrix. In (Maclaren et al., 2016), a hierarchical Bayesian approach is taken to frame the inverse problem, and a generic sampling method is used to solve the resulting problem; in (Cui et al., 2011) a more sophisticated sampling scheme is developed based on using a reduced-order (lower fidelity) model. The present work is based on extending the hierarchical Bayesian framework of (Maclaren et al., 2016) to explicitly use reduced-order models, while still allowing simple and generic sampling schemes to be used. Related work in the area of petroleum engineering and groundwater management is briefly discussed below; again, however, these do not generally take a fully Bayesian approach in the sense of carrying out MCMC sampling for fully non-linear models.

1.2.1 Hierarchical Bayesian Inference

Hierarchical Bayesian inference provides a natural, flexible and probabilistic setting in which to consider both parameter inference and predictive inference. As discussed above, rather than just providing one set of estimated model parameters, and accompanying model predictions, Bayesian inference provides probability distributions over estimates and predictions. In addition, the hierarchical framework allows assumptions on different model components, and their combinations, to be naturally formulated using standard conditional and/or marginal probability expressions: each assumption is represented by replacing a joint distribution by a factorisation in terms of simpler conditional and/or marginal distributions. This flexibility allows a number of useful approximations or modelling assumptions to be directly incorporated into the framework. There are a number of other, often closely related, approaches to formulating inverse problems

in terms of statistics, see, for example, (Evans and Stark, 2002; Kaipio and Somersalo, 2005; Stuart, 2010; Tarantola, 2004). Terminology can vary; we use ‘hierarchical Bayes’ in the sense of (Berliner, 1996, 2003,1), and this approach is discussed in detail in the next section.

A benefit of the hierarchical approach is that the problem statement and problem solution method are clearly separated. This means that the hierarchical framework can be combined with simple ‘out-of-the-box’ Markov chain Monte Carlo (MCMC) sampling tools such as emcee (Foreman-Mackey et al., 2013), Stan (Carpenter et al., 2017), or PyMC (Patil et al., 2010) for example. This was the approach taken in (Maclaren et al., 2016), where we used a hierarchical Bayesian framework to pose the inverse and prediction problems for a simple geothermal model, and then solved them via sampling using emcee. As is common when using MCMC for large models, we quickly reached the limits of computational feasibility. In principle, the hierarchical approach provides a clear way to incorporate lower-dimensional approximations of larger-scale problems so that standard MCMC sampling could remain feasible, but we did not implement this in our previous work. Thus one of our main goals here is to demonstrate how to incorporate reduced-order models into the hierarchical framework.

An alternative approach is to adopt more sophisticated sampling methods (as in Cui et al., 2011, discussed further below) but these typically require quite specialised knowledge, access to model solver information that may not be available from many solvers and/or still require reduced-order models. While the hierarchical approach is compatible with these more sophisticated sampling methods, in the present work we argue that it can already provide much of the speed-up benefit in a transparent manner without *requiring* these more sophisticated solution methods.

1.2.2 Bayesian Approximation Error

The key to the method proposed here is incorporating a model of the discrepancy between an accurate and a reduced-order model as a component in our hierarchical framework, by adapting the Bayesian approximation error (BAE) method (Kaipio and Kolehmainen, 2013; Kaipio and Somersalo, 2005). This allows us to account for modelling errors when using reduced-order models, and hence speed up computation while avoiding overconfidence in biased parameter estimates.

The standard BAE idea was first used in (Kaipio and Somersalo, 2005) and (Kaipio and Somersalo, 2007) to account for errors induced by using a reduced accuracy discretisation for the forward model in electrical impedance tomography. Since then, the method has been used to account for numerous types of model discrepancies in various applications, see, for example, (Huttunen and Kaipio, 2009; Kaipio and Kolehmainen, 2013; Kolehmainen et al., 2009; Lehtikoinen et al., 2010; Nicholson et al., 2018; Nissinen et al., 2008; Pulkkinen et al., 2016; Tarvainen et al., 2010).

In contrast to the usual BAE approach, in the present work we a) incorporate the discrepancy model into the hierarchical framework we presented in (Maclaren et al., 2016), and b) use the idea of posterior, as opposed to prior, model approximation errors. Using posterior approximation errors increases computational stability and feasibility for difficult forward problems, and also makes our error estimates more relevant to the posterior target. It does, however, come with some risk when the reduced-order, or coarse, model is a sufficiently bad approximation to the more accurate model. This is discussed further in Appendix B.

Most of the BAE literature focuses on finding MAP solutions, and we are not aware of approaches combining MCMC and BAE, other than (Cui et al., 2011) where BAE ideas were incorporated directly into the sampling scheme itself. Our earlier work (Maclaren et al., 2016) combined MCMC with a hierarchical framework but, while model approximation error was initially allowed for, in principle, it was not explicitly accounted for in the actual problem. Besides the BAE approach, there are a number of related methods for accounting for model discrepancy between accurate and simplified models, in particular with application to the management of petroleum reservoirs and groundwater systems (which present similar challenges to those of geothermal systems). A number of these approaches are discussed in (Doherty and Christensen, 2011), where the phrase *paired simple and complex models* is used to describe this general setting. These authors also introduce a theoretical analysis framework for paired models based on linear algebra. Other examples, mainly in the context of applications to petroleum reservoirs, include (Aanonsen, 2005; Kennedy and O’Hagan, 2000; Lødøen and Omre, 2008; Trehan and Durlofsky, 2018). Our focus here is on introducing a simple yet general framework to enable MCMC sampling for arbitrary simulation models, without requiring linearity assumptions on the simulation model, or requiring nonparametric statistical models.

1.2.3 Improved Sampling Schemes

The method developed in (Cui et al., 2011) is based on using an adaptive delayed acceptance Metropolis-Hastings (ADAMH) algorithm, with incorporation of model discrepancies, to carry out MCMC sampling. The ADAMH method is based on constructing the statistics of the model discrepancies adaptively on the fly. Besides basing sampling on a reduced (and hence much cheaper) model, a major benefit of this approach is that the statistics of the model discrepancies are computed over the posterior density rather than the prior density, in contrast to the standard BAE approach. There are some potential drawbacks to the method, however. Firstly, as the discrepancies are constructed on the fly, the number of accurate simulations required cannot be established a priori. Secondly, the method is quite complicated to implement for the general practitioner. These benefits and drawbacks of the method proposed in (Cui et al., 2011) provide important motivation for the current paper. We aim to develop a simple-to-use method in which calculation of the model discrepancies can be carried out efficiently, with all steps involving fine model simulations perfectly parallelizable, while also drawing the samples from a better-informed density than the prior.

1.3 Hierarchical Bayes with Posterior Model Discrepancy

In the present work, we incorporate BAE assumptions into a hierarchical framework by replacing an intractable conditional probability distribution with a simpler marginal distribution or, equivalently, by replacing an intractable joint distribution by the product of two marginal distributions. This idea has similarities with, for example, composite likelihood methods (reviewed in Varin, 2008; Varin et al., 2011), though here we focus on the BAE and hierarchical Bayesian perspectives.

With these approximations incorporated into a formalised hierarchical model, we find that standard MCMC sampling becomes much more feasible for larger models, without introducing the overconfidence in results that typically accompany the naive use of a reduced-order model. To illustrate this, we revisit a relatively simple geothermal reservoir problem that we analysed previously, and show how to extend our results to be applicable to a much finer-scale and more computationally demanding model. This enables us to carry out MCMC sampling in a day or so for a problem which would otherwise require around a year or more. We also compare the results obtained by MCMC sampling

when naively using a reduced model without BAE corrections, with those obtained by using a reduced model with BAE incorporated. Both methods require effectively the same amount of computation time, though the BAE approach requires some additional initial computation to construct the model error statistics. This additional computation is valuable however, since only using the naive reduced-order model results in overoptimistic and biased posteriors for which the known true parameters lie outside of the bulk of the support.

2 Hierarchical Framework

2.1 Key Ingredients

The main ingredients of our hierarchical Bayesian approach here are: a fine, or accurate, simulation model, represented by a function $f(\mathbf{k}_{\text{fine}})$, and a coarse, or less accurate, model, represented by a function $g(\mathbf{k}_{\text{coarse}})$. Here \mathbf{k}_{fine} and $\mathbf{k}_{\text{coarse}}$ are the (vectors of) fine- and coarse-scale parameters of interest; in our case the fine-scale and coarse-scale parameters will have the same dimension, despite corresponding to different discretisation grids, and so we will drop the explicit distinction between \mathbf{k}_{fine} and $\mathbf{k}_{\text{coarse}}$ in what follows and simply refer to both by \mathbf{k} (but see Appendix A for a discussion of the relationship between fine-scale and coarse-scale parameter grids). As discussed below, our parameters of interest here are rock permeabilities; though we work with log permeabilities throughout, for simplicity we will generally just refer to these as ‘permeabilities’.

The two models, f and g , are combined with a measurement model and a prior parameter model, as discussed below. Typically the coarse model is much cheaper to evaluate than the fine model: we wish to use the coarse model, instead of the more expensive model, for the most expensive inversion steps, while also correcting for the bias and overconfidence that arises from using the cheaper model.

2.2 Formulation

2.2.1 Hierarchical Framework

As described in (Maclaren et al., 2016), the hierarchical Bayesian approach generally begins by assuming the three-stage decomposition of a full joint probability distribution over all quantities of interest:

$$\begin{aligned}
& p(\text{observed data, process variable, process parameters, observation parameters}) \\
& = \\
& p(\text{observed data} \mid \text{process variable, observation parameters}) \\
& \times \\
& p(\text{process variable} \mid \text{process parameters}) \\
& \times \\
& p(\text{process parameters, observation parameters}).
\end{aligned} \tag{1}$$

This particular decomposition is not an identity, and instead contains plausible physical *modelling* assumptions about the conditional independencies separating measurement and process variables. For example, the measurement model (first factor) is assumed to be independent of the process parameters, while the process model (second factor) is assumed to be independent of the observation parameters. In terms of our current problem variables this becomes

$$p(\mathbf{y}_{\text{obs}}, \mathbf{y}_{\text{process}}, \mathbf{k}) = p(\mathbf{y}_{\text{obs}} \mid \mathbf{y}_{\text{process}}) p(\mathbf{y}_{\text{process}} \mid \mathbf{k}) p(\mathbf{k}), \tag{2}$$

where \mathbf{y}_{obs} is the observable (hence noisy) data vector, $\mathbf{y}_{\text{process}}$ is the latent or ‘true’ process vector, and we have suppressed the error parameters and distribution subscripts in each stage for simplicity. The model approximation error enters into the above scheme as a probabilistic process error. Intuitively, we use a probabilistic model to capture the additional uncertainty introduced by using an approximate model in place of a more accurate model. This is despite the fact that both models are deterministic; we explain the nature of this approximation in what follows.

2.2.2 Bayesian Model Approximation Error

To model the process approximation error, we first take the true or latent process variable to be generated exactly by the fine-scale model, i.e.

$$\mathbf{y}_{\text{process}} = f(\mathbf{k}). \tag{3}$$

In (Maclaren et al., 2016) we only used one model and essentially had $p(\mathbf{y}_{\text{process}}|\mathbf{k}) = \delta(\mathbf{y}_{\text{process}} - g(\mathbf{k}))$ as our process model. We carried out inference for the associated permeabilities, without taking into account knowledge of the finer-scale process model f .

Here we explicitly introduce both fine and coarse models and take into account that $p(\mathbf{y}_{\text{process}}|\mathbf{k}) \neq \delta(\mathbf{y}_{\text{process}} - g(\mathbf{k}))$. Instead, as indicated above, we have $p(\mathbf{y}_{\text{process}}|\mathbf{k}) = \delta(\mathbf{y}_{\text{process}} - f(\mathbf{k}))$. To do this, we define the process model error variable by

$$\boldsymbol{\varepsilon} = \mathbf{y}_{\text{process}} - g(\mathbf{k}) = f(\mathbf{k}) - g(\mathbf{k}). \quad (4)$$

Since both f and g are deterministic, at this point $\boldsymbol{\varepsilon}$ must be too; this can be formally incorporated into the hierarchical model by again treating deterministic functions as delta distributions. Thus we can write

$$p_{Y_p|K}(\mathbf{y}_{\text{process}}|\mathbf{k}) = p_{\boldsymbol{\varepsilon}|K}(\mathbf{y}_{\text{process}} - g(\mathbf{k})|\mathbf{k}) = p_{\boldsymbol{\varepsilon}|K}(f(\mathbf{k}) - g(\mathbf{k})|\mathbf{k}) = p_{\boldsymbol{\varepsilon}|K}(\boldsymbol{\varepsilon}|\mathbf{k}), \quad (5)$$

which simply amounts to a deterministic change of variables (carried out, e.g., via the delta method (Au and Tam, 1999; Khuri, 2004)).

The central issue we face here is that both the probabilistic process model $p_{Y_p|K}(\mathbf{y}_{\text{process}}|\mathbf{k})$ and error model $p_{\boldsymbol{\varepsilon}|K}(\boldsymbol{\varepsilon}|\mathbf{k})$ are typically intractable to simulate from for more than a limited number of realisations, as both involve the expensive fine-scale model. Thus at this stage we introduce approximations to these distributions. Importantly, our goal is not to accurately estimate the model error as such, but to approximately model the effect of marginalising over it. This is for the purpose of reducing the bias/overconfidence in parameter estimates that would result from just using the simpler model directly; some loss of precision/statistical efficiency is expected.

The basic BAE approach (Kaipio and Kolehmainen, 2013; Kaipio and Somersalo, 2005) is to first simulate a limited number of realisations from the *true* (i.e. involving the fine-scale model) joint distribution

$$p_{\boldsymbol{\varepsilon}, K}(\boldsymbol{\varepsilon}, \mathbf{k}) = p_{\boldsymbol{\varepsilon}|K}(\boldsymbol{\varepsilon}|\mathbf{k})p_K(\mathbf{k}) \quad (6)$$

using a given parameter prior $p_K(\mathbf{k})$, and then fit an approximate distribution $\hat{p}_{\boldsymbol{\varepsilon}, K}(\boldsymbol{\varepsilon}, \mathbf{k})$ to the $(\boldsymbol{\varepsilon}, \mathbf{k})$ realisations. This empirically-estimated approximate distribution is then

used as a plug-in replacement

$$p_{\mathcal{E},K}(\boldsymbol{\varepsilon}, \mathbf{k}) \stackrel{\text{plug}}{\leftarrow} \hat{p}_{\mathcal{E},K}(\boldsymbol{\varepsilon}, \mathbf{k}) \quad (7)$$

in the hierarchical model. While the true points will lie on a curve of zero thickness, \hat{p} is estimated within a non-degenerate family of probability distributions, such as a bivariate normal distribution. This procedure aims to ‘conservatively’ cover the sample points, despite the obvious model mis-specification (see Figure B.1).

An alternative approximation is often used, called the ‘enhanced error model’ in the BAE literature (Kaipio and Kolehmainen, 2013; Kaipio and Somersalo, 2005), which we will follow in the present work. This amounts to replacing the true joint distribution by the product of the empirically-estimated – but true – marginal distributions:

$$p_{\mathcal{E},K}(\boldsymbol{\varepsilon}, \mathbf{k}) \stackrel{\text{plug}}{\leftarrow} p_{\mathcal{E}}(\boldsymbol{\varepsilon})p_K(\mathbf{k}) \quad (8)$$

where

$$p_{\mathcal{E}}(\boldsymbol{\varepsilon}) = \int p_{\mathcal{E}|K}(\boldsymbol{\varepsilon}|\mathbf{k})p_K(\mathbf{k})d\mathbf{k}, \quad (9)$$

which is estimated empirically based on samples as described in Section 2.4. In the above, estimation of $p_{\mathcal{E}}(\boldsymbol{\varepsilon})$, $p_{\mathcal{E}|K}(\boldsymbol{\varepsilon}|\mathbf{k})$ is taken as the *true* conditional error distribution, and hence the samples are used to estimate the *true* marginal. On the other hand, in all subsequent calculations the joint distribution is approximated by the product of the marginals. This is equivalent to using the marginal error distribution for $\boldsymbol{\varepsilon}$ as a plug-in empirical estimator of the conditional error distribution for $\boldsymbol{\varepsilon}|\mathbf{k}$ in the hierarchical model, prior to subsequent inference steps. As emphasised above, the goal is not to get the error exact, but to account for it in a somewhat ‘conservative’ manner. While in the BAE literature this is referred to as the enhanced error model, the replacement of an intractable conditional distribution in a product of distributions by a more accessible marginal distribution is also similar in philosophy to that used in, for example, the composite likelihood literature (Varin, 2008; Varin et al., 2011). Hence we will also refer to it as the *composite* error model.

Finally, we note that *after* both the true marginal process model error has been empirically estimated and the plug-in replacement has been made for the conditional distribution, we will assume that the full process model error distribution is (formally) conditionally independent of the parameter in any subsequent manipulations of the probability distributions.

2.2.3 Posterior Model Approximation Error

A practical issue with both of the above approximation procedures (i.e. both the full and the enhanced/composite error models) arises in complicated models such as those in geothermal reservoir modelling: model run failures, long model run times and/or extreme model outputs when sampling from an insufficiently informative prior and running the fine-scale model (in particular). We encountered a large number of such model run issues for the fine-scale model and were thus motivated to consider a further approximation to the process model error. This can be described as a *posterior* plug-in estimate of the model approximation error. In particular, we make the plug-in estimate

$$p_{\mathcal{E}}(\boldsymbol{\varepsilon}) \stackrel{\text{plug}}{\leftarrow} \hat{p}_{\mathcal{E}|Y_o}(\boldsymbol{\varepsilon}|\mathbf{y}_{\text{obs}}), \quad (10)$$

where we now use the coarse-model posterior for the parameters to estimate the error distribution marginalised over the parameter. That is, we use

$$\hat{p}_{\mathcal{E}|Y_o}(\boldsymbol{\varepsilon}|\mathbf{y}_{\text{obs}}) = \int p_{\mathcal{E}|K}(\boldsymbol{\varepsilon}|\mathbf{k})\hat{p}_{K|Y_o}(\mathbf{k}|\mathbf{y}_{\text{obs}})d\mathbf{k} \quad (11)$$

which is estimated empirically based on samples as described in Section 2.4, and where

$$\hat{p}_{K|Y_o}(\mathbf{k}|\mathbf{y}_{\text{obs}}) \propto \hat{p}_{Y_o|K}(\mathbf{y}_{\text{obs}}|\mathbf{k})p(\mathbf{k}) \quad (12)$$

and $\hat{p}_{Y_o|K}$ is the likelihood function based on the coarse-scale model $g(\mathbf{k})$. Since we did not encounter model run issues in the coarse model we can estimate this by combining the likelihood with the broad prior.

Once the error distribution has been estimated we again use it in the ‘enhanced’ or ‘composite’ model of the joint distribution, along with the original prior:

$$p_{\mathcal{E},K}(\boldsymbol{\varepsilon}, \mathbf{k}) \stackrel{\text{plug}}{\leftarrow} p_{\mathcal{E}}(\boldsymbol{\varepsilon})p_K(\mathbf{k}). \quad (13)$$

Thus we are simply using a different plug-in estimate of the model error. Since this is now used with the coarse model we can revert to the broad prior without model run failures in all subsequent calculations.

Again, because our goal is not to model the error exactly, but rather to model the effect of marginalising over it, we are willing to tolerate more potential inaccuracies at this stage. The present step of using posterior sampling for the discrepancy is ‘riskier’ than that in the previous section, however, in the sense that it involves a formal ‘dou-

ble use of data’ and tends to *narrow* rather than widen the error distribution, when compared to the distribution that results from using the prior. This is also apparent from the replacement of a marginal distribution by a conditional distribution (conditional on the observations), rather than the usual replacement of a marginal distribution by a conditional distribution. We are still ultimately replacing a deterministic function by a probabilistic model, however.

A geometric interpretation of this posterior model approximation step, and its potential dangers, is given in Appendix B. Despite these warnings we believe that it is often a practical solution in complex models, and does have the benefit of providing more ‘relevant’ estimates of the model error when the posterior based on the coarse model is not too far from the true posterior. One way to check this assumption would be to recompute the model error distribution under the final posterior and compare it to the error distribution computed under the coarse model posterior; checking for similarity of these distributions can be thought of as a form of posterior predictive check. This check does, however, require recomputing realisations from the fine-scale model and so is not always practical.

2.2.4 Completion of the Hierarchical Model

Our measurement model is assumed to take the form

$$p_{Y_o|Y_p}(\mathbf{y}_{\text{obs}}|\mathbf{y}_{\text{process}}) = p_{E|Y_p}(\mathbf{y}_{\text{obs}} - \mathbf{y}_{\text{process}}|\mathbf{y}_{\text{process}}) = p_E(\mathbf{y}_{\text{obs}} - \mathbf{y}_{\text{process}}) = p_E(e). \quad (14)$$

Here

$$e = \mathbf{y}_{\text{obs}} - \mathbf{y}_{\text{process}}, \quad (15)$$

where $e \sim p_{E|Y_p}(\cdot) = p_E(\cdot)$ due to our independence assumptions.

Combining the error models, and introducing the total error term $\nu = \boldsymbol{\varepsilon} + e$, leads to

$$\mathbf{y}_{\text{obs}} = g(\mathbf{k}) + \boldsymbol{\varepsilon} + e = g(\mathbf{k}) + \nu. \quad (16)$$

2.3 Posterior Target

Our goal here is to compute the posterior for the parameters given the data

$$p(\mathbf{k}|\mathbf{y}_{\text{obs}}) \propto p(\mathbf{y}_{\text{obs}}|\mathbf{k})p(\mathbf{k}), \quad (17)$$

where the process model (or process model error) has been marginalised over, and where $p(\mathbf{y}_{\text{obs}}|\mathbf{k})$ is called the likelihood and $p(\mathbf{k})$ is called the prior. The likelihood can be obtained by formal marginalisation over the total error via

$$\begin{aligned}
p_{Y_o|K}(\mathbf{y}_{\text{obs}}|\mathbf{k}) &= \int p_{Y_o, \mathcal{V}|K}(\mathbf{y}_{\text{obs}}, \nu|\mathbf{k})d\nu = \int p_{Y_o|\mathcal{V}, K}(\mathbf{y}_{\text{obs}}|\mathbf{k}, \nu)p_{\mathcal{V}|K}(\nu|\mathbf{k})d\nu \\
&= \int \delta(\mathbf{y}_{\text{obs}} - g(\mathbf{k}) - \nu)p_{\mathcal{V}|K}(\nu|\mathbf{k})d\nu \\
&= p_{\mathcal{V}|K}(\mathbf{y}_{\text{obs}} - g(\mathbf{k})|\mathbf{k}) \\
&= p_{\mathcal{V}}(\mathbf{y}_{\text{obs}} - g(\mathbf{k})),
\end{aligned} \tag{18}$$

where the last step follows from the (formal) independence of both error models from the parameter.

The above steps can also simply be considered as a change of variables from $Y_o|K$ to $\mathcal{V}|K$ via the delta method (Au and Tam, 1999; Khuri, 2004). Thus the posterior can be written as

$$\begin{aligned}
p_{K|Y_o}(\mathbf{k} | \mathbf{y}_{\text{obs}}) &\propto p_{Y_o|K}(\mathbf{y}_{\text{obs}}|\mathbf{k})p_K(\mathbf{k}) \\
&= p_{\mathcal{V}|K}(\mathbf{y}_{\text{obs}} - g(\mathbf{k})|\mathbf{k})p_K(\mathbf{k}) \\
&= p_{\mathcal{V}}(\mathbf{y}_{\text{obs}} - g(\mathbf{k}))p_K(\mathbf{k}),
\end{aligned} \tag{19}$$

where again the last step follows from the formal conditional independence structures of the error distributions.

The process error has now been absorbed into the likelihood, and the resulting expression is simply a standard ‘measurement’ likelihood function, written in terms of total error, multiplied by the prior. It does, however, require the distribution of the total error, $p_{\mathcal{V}}(\cdot)$, to be known. At this point, we a) assume that the measurement error e is Gaussian and b) approximate the process model error ε as Gaussian. This makes combining these two errors straightforward (as described in the next subsection). Ultimately, we determine whether these, and the other approximations used thus far, are reasonable based on whether they work in practice – e.g. whether they recover good estimates of the true parameters in test cases, and whether any available error distributions ‘look normal’ when plotted (or, if desired, pass formal tests of normality).

2.4 Constructing the Statistics of the Total Errors

By taking a Gaussian approximation of the process error we can characterise its distribution with the mean and covariance only. These cannot be computed analytically in general, and thus must be estimated empirically via samples. In this section we give a brief review of the standard *enhanced/composite error model* approach and also outline the proposed *posterior-sampled enhanced/composite error model* approach. Pseudocode algorithms are provided for both of the methods.

2.4.1 The Standard Enhanced/Composite Error Model Approach

To calculate the statistics of the the process error, $\boldsymbol{\varepsilon}$, in the standard enhanced/composite error model approach, an ensemble of $q \in \mathbb{N}$ samples are drawn from the prior distribution $p(\mathbf{k})$, say $\mathbf{k}^{(\ell)}$, for $\ell = 1, 2, \dots, q$. Both the fine and coarse models are then run for these samples, resulting in an ensemble of discrepancies

$$\boldsymbol{\varepsilon}^{(\ell)} = f(\mathbf{k}^{(\ell)}) - g(\mathbf{k}^{(\ell)}). \quad (20)$$

The ensemble mean and covariance of the model discrepancies are then estimated using

$$\boldsymbol{\varepsilon}_* = \frac{1}{q} \sum_{\ell=1}^q \boldsymbol{\varepsilon}^{(\ell)}, \quad \boldsymbol{\Gamma}_{\boldsymbol{\varepsilon}} = \frac{1}{q-1} \sum_{\ell=1}^q (\boldsymbol{\varepsilon}^{(\ell)} - \boldsymbol{\varepsilon}_*)(\boldsymbol{\varepsilon}^{(\ell)} - \boldsymbol{\varepsilon}_*)^T. \quad (21)$$

As discussed above, the total error, ν , is the sum of both the noise and the process model error, and thus the distribution for the total error is given by

$$\nu \sim \mathcal{N}(\nu_*, \boldsymbol{\Gamma}_{\nu}) = \mathcal{N}(e_* + \boldsymbol{\varepsilon}_*, \boldsymbol{\Gamma}_e + \boldsymbol{\Gamma}_{\boldsymbol{\varepsilon}}). \quad (22)$$

This new distribution is then used to update the likelihood density, which consequently updates the posterior density.

Algorithm 1 gives pseudocode for the standard enhanced/composite error model approach for constructing the distribution of the total errors and for carrying out the inversion.

Algorithm 1 The standard *enhanced/composite error model* approach

draw $\mathbf{k}^{(1)}, \mathbf{k}^{(2)}, \dots, \mathbf{k}^{(q)}$ from the prior, $p(\mathbf{k})$
 set $\boldsymbol{\varepsilon}^{(\ell)} = f(\mathbf{k}^{(\ell)}) - g(\mathbf{k}^{(\ell)})$ for $\ell = 1, 2, \dots, q$
 calculate $\boldsymbol{\varepsilon}_* = \frac{1}{q} \sum_{\ell=1}^q \boldsymbol{\varepsilon}^{(\ell)}$ and $\Gamma_{\boldsymbol{\varepsilon}} = \frac{1}{q-1} \sum_{\ell=1}^q (\boldsymbol{\varepsilon}^{(\ell)} - \boldsymbol{\varepsilon}_*)(\boldsymbol{\varepsilon}^{(\ell)} - \boldsymbol{\varepsilon}_*)^T$
 set $\nu = \boldsymbol{\varepsilon} + e$ with $\nu \sim \mathcal{N}(\nu_*, \Gamma_{\nu}) = \mathcal{N}(\boldsymbol{\varepsilon}_* + e_*, \Gamma_{\boldsymbol{\varepsilon}} + \Gamma_e)$
 replace the likelihood $p_E(\mathbf{y}_{\text{obs}} - f(\mathbf{k}))$ with $p_{\nu}(\mathbf{y}_{\text{obs}} - g(\mathbf{k}))$
 use MCMC to sample the new posterior $\propto p_{\nu}(\mathbf{y}_{\text{obs}} - g(\mathbf{k}))p(\mathbf{k})$, based on the
 new likelihood and original prior

2.4.2 The Proposed Posterior-Sampled Enhanced/Composite Error Model Approach

In the proposed approach we avoid sampling from the prior density of \mathbf{k} to generate the ensemble $\boldsymbol{\varepsilon}^{(\ell)}$. Instead, we initially construct a *naive posterior* density of \mathbf{k} , $\hat{p}(\mathbf{k}|\mathbf{y}_{\text{obs}})$ using MCMC with the likelihood function induced by the noise term, e , only. This results in samples from the naive posterior, $\mathbf{k}^{(\ell)}$, which are then passed through the two models to construct the process model errors, $\boldsymbol{\varepsilon}^{(\ell)}$. Once these samples for $\boldsymbol{\varepsilon}$ have been generated, the method is essentially the same as that of the standard enhanced/composite error model approach.

Pseudocode for the proposed posterior-sampled enhanced/composite error model approach is given in Algorithm 2.

Algorithm 2 The proposed *posterior-sampled enhanced/composite error model* approach

use MCMC to obtain samples $\mathbf{k}^{(1)}, \dots, \mathbf{k}^{(q)}$ from the naive posterior,
 $\hat{p}(\mathbf{k}|\mathbf{y}_{\text{obs}})$, based on the coarse model g
 set $\boldsymbol{\varepsilon}^{(\ell)} = f(\mathbf{k}^{(\ell)}) - g(\mathbf{k}^{(\ell)})$ for $\ell = 1, 2, \dots, q$
 calculate $\boldsymbol{\varepsilon}_* = \frac{1}{q} \sum_{\ell=1}^q \boldsymbol{\varepsilon}^{(\ell)}$ and $\Gamma_{\boldsymbol{\varepsilon}} = \frac{1}{q-1} \sum_{\ell=1}^q (\boldsymbol{\varepsilon}^{(\ell)} - \boldsymbol{\varepsilon}_*)(\boldsymbol{\varepsilon}^{(\ell)} - \boldsymbol{\varepsilon}_*)^T$
 set $\nu = \boldsymbol{\varepsilon} + e$ with $\nu \sim \mathcal{N}(\nu_*, \Gamma_{\nu}) = \mathcal{N}(\boldsymbol{\varepsilon}_* + e_*, \Gamma_{\boldsymbol{\varepsilon}} + \Gamma_e)$
 replace the likelihood $p_E(\mathbf{y}_{\text{obs}} - f(\mathbf{k}))$ with $p_{\nu}(\mathbf{y}_{\text{obs}} - g(\mathbf{k}))$
 use MCMC to sample the new posterior $\propto p_{\nu}(\mathbf{y}_{\text{obs}} - g(\mathbf{k}))p(\mathbf{k})$, based on the
 new likelihood and original prior

3 Computational Methods

3.1 The Forward Model

3.1.1 Governing Equations

The governing forward problem we consider is multiphase nonisothermal flow in a two-dimensional geothermal reservoir. This general problem is governed by the mass balance and the energy balance equations:

$$\frac{d}{dt} \int_{\Omega} M_m dV = - \int_{\partial\Omega} \mathbf{F}_m \cdot \mathbf{n} dS + \int_{\Omega} q_m dV \quad (23)$$

and

$$\frac{d}{dt} \int_{\Omega} M_e dV = - \int_{\partial\Omega} \mathbf{F}_e \cdot \mathbf{n} dS + \int_{\Omega} q_e dV, \quad (24)$$

respectively (Pruess et al., 1999). Here Ω is the control volume with boundary $\partial\Omega$, \mathbf{n} denotes an outward pointing normal vector to $\partial\Omega$, M_m and M_e represent amount of mass per unit volume and amount of energy per unit volume respectively, \mathbf{F}_m and \mathbf{F}_e are the mass flux and energy flux respectively, while q_m and q_e represent mass sinks or sources and energy sinks or sources respectively.

We consider observations of temperature only, while the parameters of interest are limited to (log) rock-type permeabilities. Other parameters which may be of interest include deep sources, relative permeabilities, and porosities, while other observable quantities include production history pressure and enthalpy. The relationship between the permeabilities and temperature, i.e. the *parameter-to-observable map*, can be understood by examining the key terms in (23) and (24), following (Cui et al., 2011). A more in-depth discussion is given in (Pruess et al., 1999). Firstly, the amount of mass and energy per unit control volume are given by

$$M_m = \phi(\rho_l S_l + \rho_v S_v), \quad (25)$$

$$M_e = (1 - \phi)\rho_r u_r T + \phi(\rho_l u_l S_l + \rho_v u_v S_v), \quad (26)$$

respectively, where ϕ is porosity, S_l is liquid saturation, S_v is vapour saturation, ρ_l is the density of the liquid, ρ_v is the vapour density, ρ_r is density of the rock, u_l is internal en-

ergy of the liquid, u_v is internal energy of the vapour, u_r is the specific heat of the rock, and T is temperature. Next, the mass flux is given by the sum of the mass flux of liquid and the mass flux of vapour,

$$\mathbf{F}_m = \mathbf{F}_{ml} + \mathbf{F}_{mv}, \quad (27)$$

where

$$\mathbf{F}_{ml} = -\frac{\mathbf{K}k_{rl}}{\nu_l}(\nabla p - \rho_l \mathbf{g}), \quad (28)$$

$$\mathbf{F}_{mv} = -\frac{\mathbf{K}k_{rv}}{\nu_v}(\nabla p - \rho_v \mathbf{g}). \quad (29)$$

Here \mathbf{K} is the permeability tensor, p is pressure, ν_l and ν_v are kinematic viscosity of liquid and vapour respectively, k_{rl} and k_{rv} are relative permeabilities, while \mathbf{g} is gravitational acceleration. Finally, the energy flux is given by

$$\mathbf{F}_e = h_l \mathbf{F}_{ml} + h_v \mathbf{F}_{mv} - K \nabla T, \quad (30)$$

where h is specific enthalpy and K is thermal conductivity. In our study, all parameters other than rock permeabilities were taken as known.

3.1.2 Model Simulation

We consider a two-dimensional slice model, shown in Figure 1, based on that considered in (Bjarkason et al., 2016) and (Maclaren et al., 2016).

To solve the forward problem we use the computer package AUTOUGH2 (Yeh et al., 2012), The University of Auckland's version of the TOUGH2 (Pruess et al., 1999) simulator, with the pure water equation of state model EOS1. We only consider steady (natural) state conditions, though we calculate steady states via time marching to assist convergence to proper model solutions.

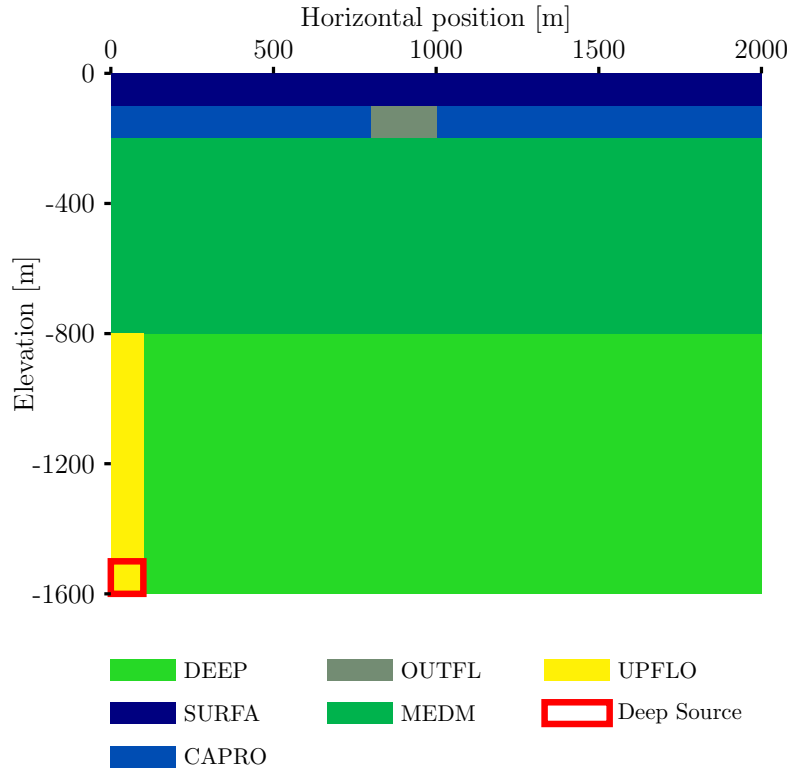


Figure 1. Rectangular slice model geometry showing the rock-type locations, independent of computational grid discretization.

The model geometry is a rectangular slice with physical dimensions of 1600 m deep and 2000 m wide. For our test problem we restricted the unknowns to a set of 12 parameters, two each for six rock-type regions, where these regions are assumed known in the present work. All six rock-types are assumed to have the same porosity (10%), rock grain density ($2,500 \text{ kg/m}^3$), thermal conductivity ($2.5 \text{ W/(m}\cdot\text{K)}$) and specific heat ($1.0 \text{ kJ/(kg}\cdot\text{K)}$). The top boundary condition consists of constant pressure of 1 atm and constant temperature of 15 deg C. The bottom boundary condition consists of a constant heat flux of 80 mW/m^2 , except at the bottom-left corner region (see Figure 1) where $7.5 \times 10^{-5} \text{ kg/(s}\cdot\text{m}^2)$ of a 1,200 kJ/kg enthalpy fluid is used as a deep source input. The side boundaries are closed.

We used two different computational discretizations, described in the following section.

3.2 Model Discrepancy Computation

3.2.1 Calculation steps

To calculate the statistics of the model discrepancy, we simulated both the fine model, $\mathbf{f}(\mathbf{k}_{\text{fine}})$, and the coarse model, $\mathbf{g}(\mathbf{k}_{\text{coarse}})$, 1000 times each using AUTOUGH2. These simulations were taken over the naive posterior, which was first generated by running MCMC for 150,000 samples using the coarse model, without accounting for the model discrepancy. The statistics of the model discrepancy were then calculated, as described above, by running the coarse and fine models on 1000 samples randomly selected from the full set of 150,000 naive posterior samples.

The fine model geometry consisted of a square grid of $81 \times 100 = 8100$ blocks (including one layer of atmospheric blocks), and the coarse model consisted of a grid of $17 \times 20 = 340$ blocks (again including one layer of atmospheric blocks). These model grids are shown in Appendix A. To ensure consistency of measurement locations we used the functionality of PyTOUGH described in (O’Sullivan et al., 2013), which allows the same observation wells to be defined independently of grid resolution. Measurements then consisted of temperatures taken at 15 depths down each of 7 vertical wells; this gave a total of $d = 105$ measurement points, see Figure A.1.

3.2.2 Timings

The fine model took approximately 1-5 minutes per simulation, while the coarse model took less than half a second per simulation, typically about 0.45 seconds. Thus generating 150,000 samples using MCMC to construct the posterior distribution using the fine model would take around 100-500 days, whereas using the same number of samples to construct the discrepancy-informed posterior using the coarse model took just less than 20 hours. Only taking into account these MCMC runs, in the worst case this represents a speed-up of at least a factor of 100.

In addition, however, the model discrepancy calculations require both a naive posterior and the model discrepancy statistics to be calculated. Approximately the same amount of time, i.e. approximately 20 hours, was required to run full MCMC for the naive case and for the discrepancy-informed case. The key computation in each case of MCMC is running the coarse model, only the statistics of the likelihood model differ. In contrast,

simulations of both the coarse and accurate model are required to calculate the model discrepancy statistics. We generated 1000 samples by running 200 runs of each in parallel on 5 nodes; this also took just under 20 hours. Thus the total time for inversions using the model discrepancy approach is approximately $20 \times 3 = 60$ hours. The worst-case effective speed-up factor is thus at least 30 in the present work, but typically more like 50-150.

Natural ways to increase the speed-up further include, for example, only running an approximate, optimization-based sampler to generate the initial naive posterior (from which only 1000 samples will be used). In our case, however, we simply ran full MCMC separately for both the naive and the discrepancy-informed cases. This enabled us to give a fair comparison of the results from these two models.

3.3 MCMC Sampling

MCMC sampling was carried out using the Python package *emcee* (Foreman-Mackey et al., 2013). This package implements an affine invariant ensemble sampler (Goodman and Weare, 2010) and has the benefit of being easy to implement for arbitrary user-defined models. It also allows for easy communication with the PyTOUGH Python interface (Croucher, 2011) to AUTOUGH2. In each case (with and without incorporation of the model discrepancy) 150,000 samples were computed (an ensemble of 300 *walkers* taking 500 samples each) after discarding an initial 30,000 *burn-in* samples. Computations were carried out on a standard desktop computer with an AMD Ryzen 5 1600 3.2GHz 6-Core Processor.

Though widely used in the astro-statistics community, in particular, some concerns have been raised about the performance of the affine invariant ensemble sampler in very high-dimensional problems (Huijser et al., 2015). Thus for problems involving more parameters than considered here, it could be worth also considering alternative out-of-the-box samplers like those available in Stan (Carpenter et al., 2017), or PyMC (Patil et al., 2010). In the case of Stan, however, access to model derivatives is also required.

3.4 Availability

Our code was written in Python 2.7 and is available from <https://github.com/omaclaren/hierarchical-bae-manuscript>. All of the Python packages used are open source, but access to the AUTOUGH2/TOUGH2

(Pruess et al., 1999; Yeh et al., 2012) simulator is also required; we plan to adapt our code to use the new open-source Waiwera simulator (Croucher et al., 2018) when it is officially released.

4 Results and Discussion

Here we compare a series of inversion results obtained under the coarse model, with and without model discrepancy incorporated into the hierarchical framework. We consider both data space (posterior predictive) and parameter space (parameter posterior) distributions.

Particular emphasis is placed on a) the feasibility of the posterior uncertainty estimates in parameter space, that is, the question of whether or not the posterior uncertainty is consistent with, i.e. supports, the true (log-) permeability values, and b) the role of predictive checks with and without model discrepancy.

4.1 Posterior Predictive Checks

In Figure 2 we show posterior predictive checks constructed by running the model on a subset of posterior samples obtained from MCMC. Realisations of the process model without measurement error are plotted in blue, while the data obtained from running the fine model and adding measurement error are shown in black. Figure 2 (a) shows the posterior predictive check under the coarse model with no model discrepancy included.

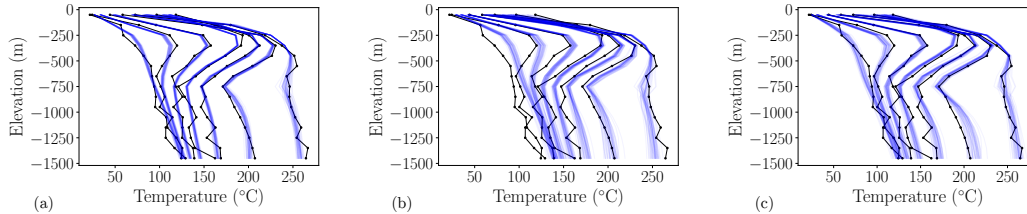


Figure 2. Posterior predictive checks for (a) the naive model without discrepancy correction, (b) only the model discrepancy error correlations included and (c) the model discrepancy errors included, with both the model error correlations and offset (bias) terms. Comparison of (b) and (c) shows that both error correlations and the bias term are important for obtaining a properly fitting model. More importantly, the difference in variation between (a) and (c) indicates that we are potentially *underestimating* the uncertainties involved in naively using the coarse model for inversion

As can be seen in the figure, the coarse model fits the data well and the uncertainties are small. Thus this check does not flag any potential issue with naively using the coarse model. On the other hand, (b) and (c) show the predictive checks resulting from inference under the discrepancy-corrected model. In particular, (b) shows the results when only the error correlations are accounted for, while (c) shows the results when both the model error correlations and offset (bias) terms are included. Comparison of (b) and (c) shows that both error correlations and the bias term are important for obtaining a properly fitting model. More importantly, the difference in variation between (a) and (c) indicates that we are potentially *underestimating* the uncertainties involved in naively using the coarse model for inversion. Intuitively, the low-variance of the posterior is counterbalanced by the introduction of additional bias into the parameter estimates. This is illustrated in the next subsection.

An implication of these results is that, in general, *posterior predictive checks against the original data do not appear to indicate issues that arise due to inversion under a reduced-order model*. One potential fix for this is to either carry out checks on held-out data or, in our case, against a more expensive/accurate model which effectively plays the role of held-out data.

4.2 Parameter Posterior Distributions

Here we consider the (marginal) parameter space posterior distributions, both for the naive and the discrepancy-informed models. Full corner plots (produced using Foreman-Mackey, 2016) are given in Appendix C.

Figures 3-8 show the marginal posteriors of the permeability for each rock-type and each direction, and both with and without incorporation of the model discrepancies. As can be seen, naive inversion under the coarse model often results in essentially infeasible parameter estimates, i.e. posteriors for which the truth is assigned only a small amount of probability density. On the other hand, the discrepancy-corrected case always assigns a large part of the posterior density to the true parameters. In reality, of course, neither model will be correct, but it is hoped that the fine-scale model is a better reflection of the truth.

Some of the parameters appear to be effectively non-identifiable, as measured by the change from prior to posterior distributions (Evans, 2015). In particular k_x^{CAPRO} and k_x^{OUTFL} appear to be largely uninformed by the data. Physically this could be explained by the fact that there is very little horizontal fluid flow in the cap rock and essentially all fluid in the outflow region is in the vertical direction. On the other hand, the remaining parameters appear to be reasonably well-identifiable; some, in particular k_y^{CAPRO} , k_x^{MEDM} , k_y^{MEDM} , k_y^{SURF} and k_y^{UPFLO} appear to be strongly identified. Under the naive model, however, inversion for the strongly identifiable parameters gives posteriors that *appear* very well-informed but are in fact providing effectively infeasible estimates. This provides another trade-off, where parameters that are strongly informed by the data under the model will be strongly incorrectly estimated under an incorrect version of the model.

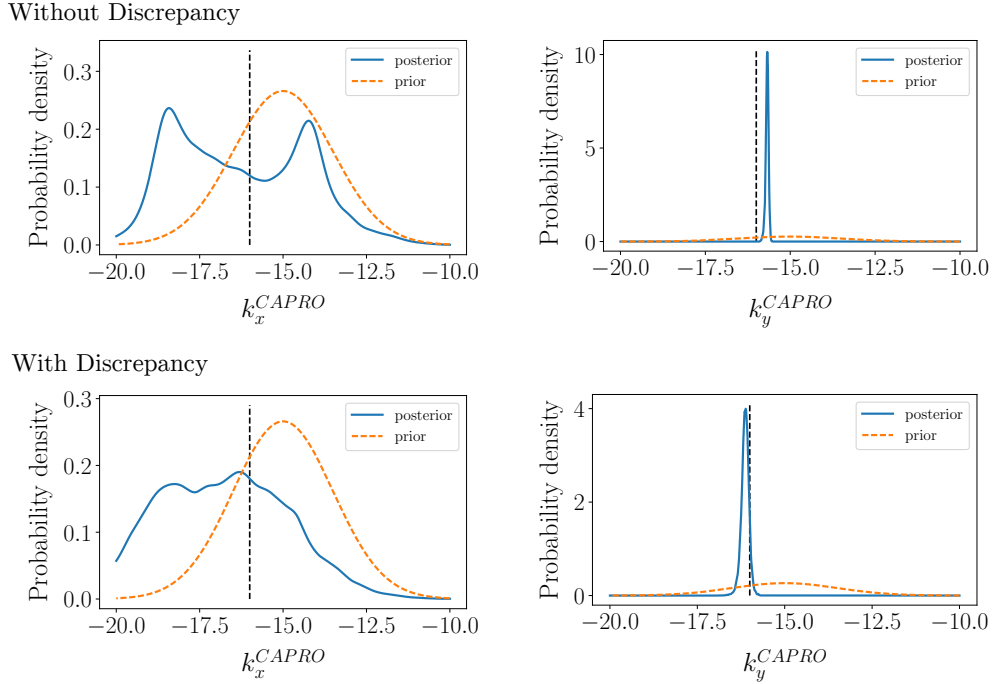
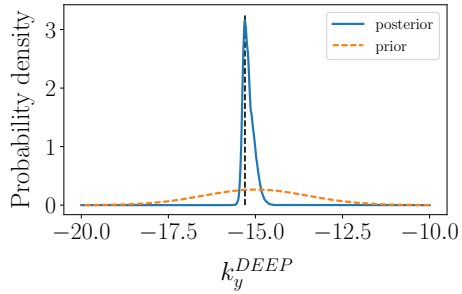
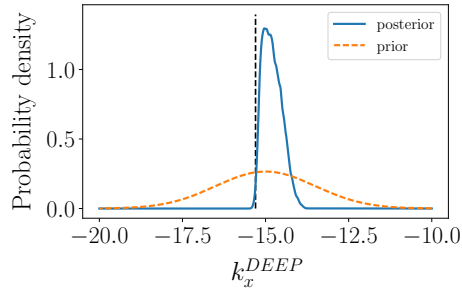


Figure 3. Marginal posteriors for cap rock (log) permeabilities, in both horizontal (x) directions (left figures) and vertical (y) directions (right figures) and for both without (top row) and with model discrepancies incorporated. The horizontal permeabilities appear to be poorly identified by the data, as measured by the change from prior to posterior distributions, while the vertical permeabilities appear strongly identified. When using the naive, i.e. non-corrected, model however, the posterior is providing effectively infeasible estimates. In contrast the discrepancy-corrected posterior covers the true parameters well in all cases.

Without Discrepancy



With Discrepancy

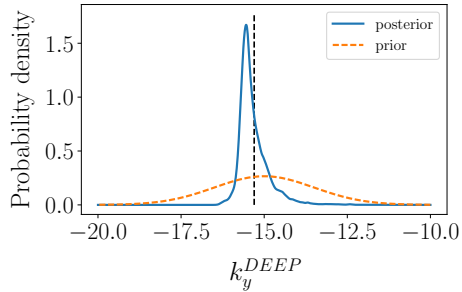
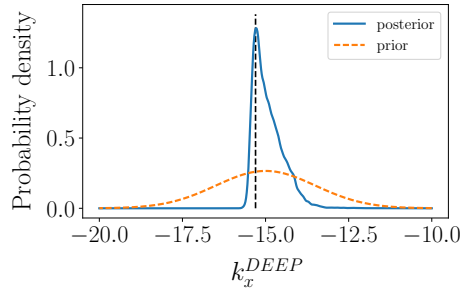
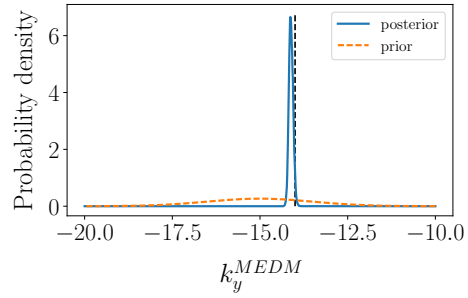
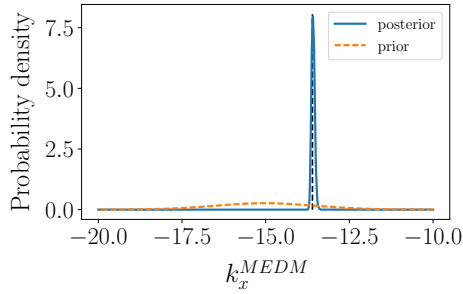


Figure 4. Marginal posteriors for deep rock (log) permeabilities, in both horizontal (x) directions (left figures) and vertical (y) directions (right figures) and for both without (top row) and with model discrepancies incorporated. Both the horizontal permeabilities and vertical permeabilities appear to be fairly well identified by the data, as measured by the change from prior to posterior distributions. When using the naive, i.e. non-corrected, model however, the posterior is providing effectively infeasible estimates, for the horizontal permeability in particular. In contrast the discrepancy-corrected posterior covers the true parameters well in all cases.

Without Discrepancy



With Discrepancy

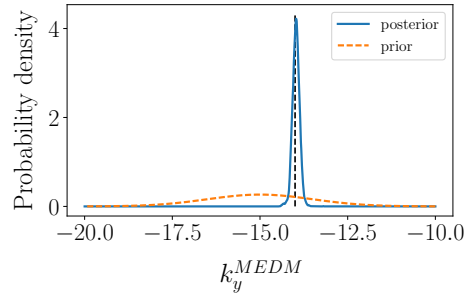
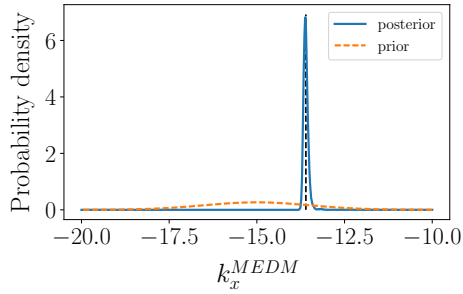


Figure 5. Marginal posteriors for medium-depth rock (log) permeabilities, in both horizontal (x) directions (left figures) and vertical (y) directions (right figures) and for both without (top row) and with model discrepancies incorporated. Both the horizontal permeabilities and vertical permeabilities appear to be strongly identified by the data, as measured by the change from prior to posterior distributions. When using the naive, i.e. non-corrected, model however, the posterior is providing effectively infeasible estimates for the vertical permeability in particular. In contrast the discrepancy-corrected posterior covers the true parameters well in all cases.

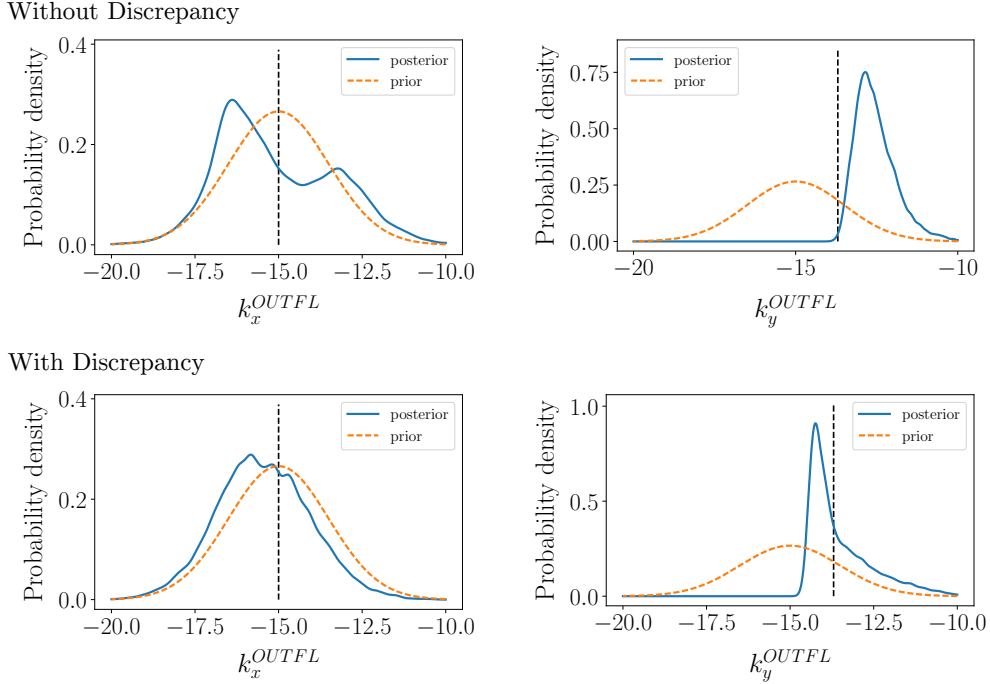
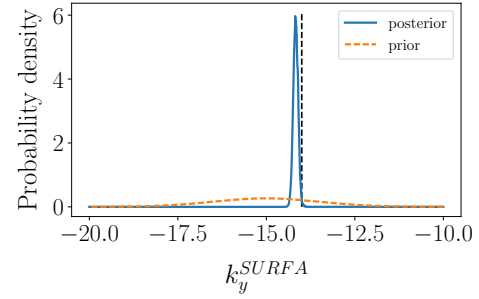
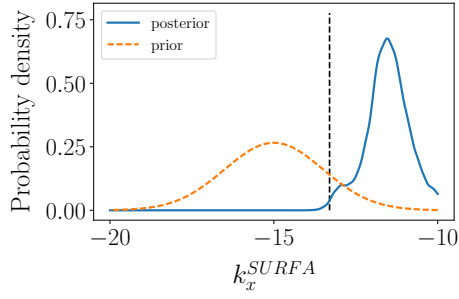


Figure 6. Marginal posteriors for outflow rock (log) permeabilities, in both horizontal (x) directions (left figures) and vertical (y) directions (right figures) and for both without (top row) and with model discrepancies incorporated. The horizontal permeabilities appear to be poorly identified by the data, as measured by the change from prior to posterior distributions, while the vertical permeabilities appear strongly identified. When using the naive, i.e. non-corrected, model however, the posterior is providing effectively infeasible estimates for the vertical permeability in particular. In contrast the discrepancy-corrected posterior covers the true parameters well in all cases.

Without Discrepancy



With Discrepancy

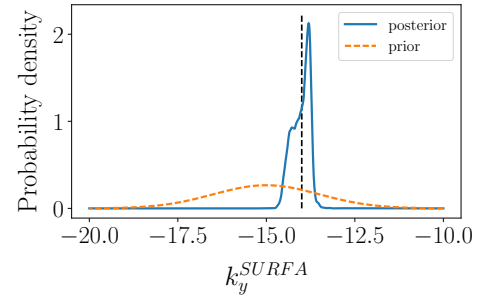
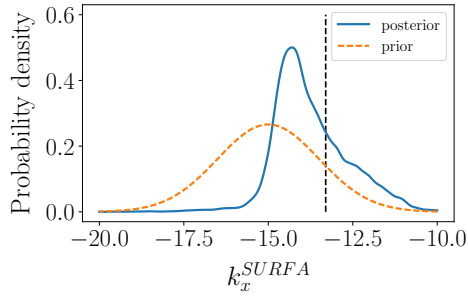


Figure 7. Marginal posteriors for surface rock (log) permeabilities, in both horizontal (x) directions (left figures) and vertical (y) directions (right figures) and for both without (top row) and with model discrepancies incorporated. Both the horizontal permeabilities and vertical permeabilities appear to be fairly well identified by the data, as measured by the change from prior to posterior distributions, vertical permeabilities in particular. When using the naive, i.e. non-corrected, model however, the posterior is providing effectively infeasible estimates for both the horizontal and vertical permeabilities. In contrast the discrepancy-corrected posterior covers the true parameters well in all cases.

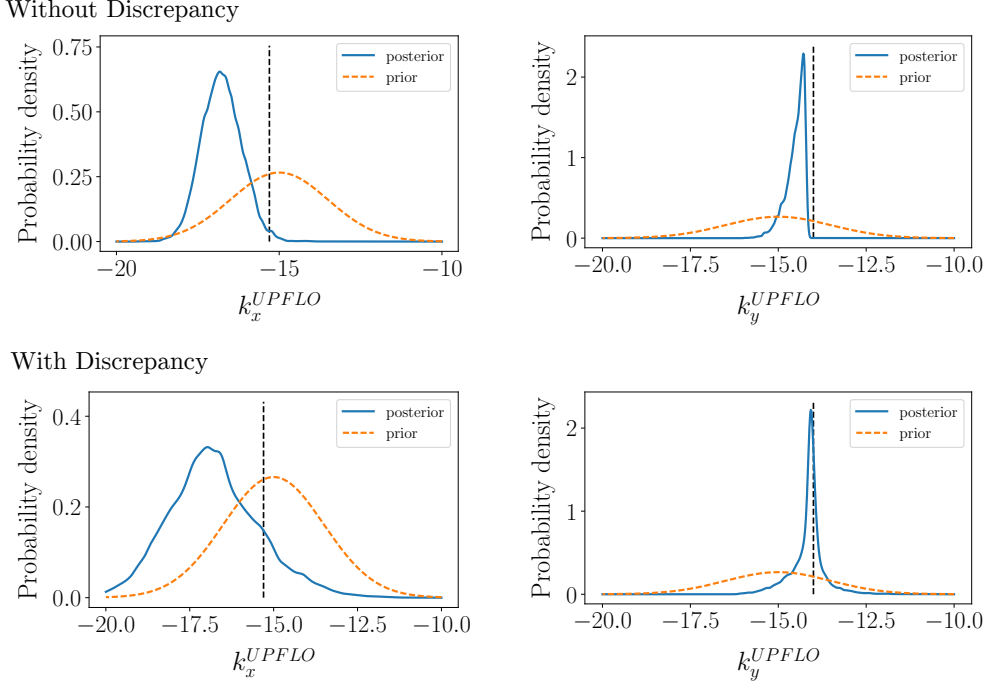


Figure 8. Marginal posteriors for upflow rock (log) permeabilities, in both horizontal (x) directions (left figures) and vertical (y) directions (right figures) and for both without (top row) and with model discrepancies incorporated. Both the horizontal permeabilities and vertical permeabilities appear to be fairly well identified by the data, as measured by the change from prior to posterior distributions, vertical permeabilities in particular. When using the naive, i.e. non-corrected, model however, the posterior is providing effectively infeasible estimates for both the horizontal and vertical permeabilities. In contrast the discrepancy-corrected posterior covers the true parameters well in all cases.

4.3 Discrepancy-corrected vs Uncorrected Approaches

The results considered above were obtained using a relatively simple geothermal reservoir problem, using both a coarse version of the model and a much finer-scale, and hence more computationally demanding, version of the model. As can be seen, standard MCMC sampling is much more computationally feasible for this problem when using a coarse model. Importantly, however, we see that just using the naive reduced-order model without discrepancy correction tends to give overconfident and biased posteriors, for which the known true parameters can lie outside of the bulk of the support. On the other hand,

the discrepancy-corrected procedure gives almost as precise estimates of the parameters, while also containing the known true parameters inside the bulk of the support in all cases.

Both methods require effectively the same amount of computation time, though the BAE approach requires some additional initial computation to construct the model error statistics. This additional computational effort is the price paid to avoid misleading estimates and is still significantly less than attempting MCMC using the fine model.

4.4 Alternatives to MCMC Sampling

In this paper we have only considered the use of MCMC to estimate the posterior density for the permeabilities, based on a discrepancy-corrected coarse model. In some settings, however, MCMC may be computationally infeasible even with the coarse model (with or without discrepancies included). In this case, the posterior model discrepancy can still be constructed without MCMC, as long as some alternative method is available for drawing the (smaller) set of required samples from the naive posterior. For example, here we only required 1000 samples from the naive posterior, compared to the 150,000 used for full MCMC runs. This would then enable the use of a discrepancy-corrected coarse surrogate model alongside alternative sampling and/or optimisation-based approaches.

5 Conclusions

We have demonstrated how to carry out simple yet computationally feasible parameter estimation and uncertainty quantification for geothermal simulation models by using a coarser, or cheaper, model in place of a finer, or more expensive, model. Our approach was to construct an approximation to the posterior Bayesian model approximation error and incorporate this into a hierarchical Bayesian framework. The hierarchical Bayesian perspective provides a flexible and intuitive setting for specifying assumptions on different model components and their combinations. In this view, approximations and modelling assumptions are directly incorporated into the framework by replacing joint distributions by factorisations in terms of simpler conditional and/or marginal distributions.

Our approach requires two simple initial computational steps in order to correct for the bias and/or overconfidence that would normally be introduced by directly using the coarse model in place of the finer model. These two steps then enable standard, out-

of-the-box MCMC to be used to sample the parameter posterior using the coarse model. We demonstrated our approach on a problem which would normally require around a year or more to run standard MCMC, and found that we could now carry out standard, out-of-the-box MCMC sampling in a day or so. This does assume, however, that MCMC is feasible using the coarse-scale model.

Our approach consists of three relatively simple steps overall and should be more accessible to general practitioners than having to manually implement more complex sampling schemes. Furthermore, the methods developed here should be generally applicable to related inverse problems such as, for example, those appearing in petroleum reservoir engineering and groundwater management.

A Mapping Between Fine and Coarse Grids

To facilitate computation of the process model error, and following (Kaipio and Kolehmainen, 2013), in this study we have been implicitly assuming that the difference between the fine and coarse models can be approximated as

$$\boldsymbol{\varepsilon} = \mathbf{y}_{\text{process}} - g(\mathbf{k}_{\text{coarse}}) = f(\mathbf{k}_{\text{fine}}) - g(\mathbf{k}_{\text{coarse}}) \approx f(\mathbf{k}_{\text{coarse}}) - g(\mathbf{k}_{\text{coarse}}) = f(\mathbf{k}) - g(\mathbf{k}). \quad (\text{A.1})$$

Here $f(\mathbf{k}_{\text{coarse}})$ is a slight abuse of notation and still in fact represents the fine model evaluated on a fine parameter grid; however the parameters are fixed to be homogeneous within a given rock-type, matching the values in the corresponding rock types on the coarser grid. Thus the parameter vectors have the same effective dimension (and values), equal to that of the coarse grid, and thus are in 1-1 correspondence. This is made clearer by comparing Figure A.1 below to Figure 1 introduced earlier: each mesh in Figure A.1 represents a different discretization of the *same* underlying parameter grid given in Figure 1. This assumption means we can compute the approximation error by sampling the coarse parameters directly rather than the (larger-dimensional) fine parameters. Implicitly, however, this is neglecting some of the approximation error that would be induced by sampling over all fine parameter sets compatible with the given coarse parameter set. This assumption can be checked/removed to the extent that computational resources allow computing the error over the fine grid (Kaipio and Kolehmainen, 2013). Either way, the *coarse* grid parameters are the ultimate targets of inference, and by using the more con-

servative ‘enhanced’ (or ‘composite’) error model based on the marginal error distribution we can hope to account for some of this additional uncertainty indirectly.

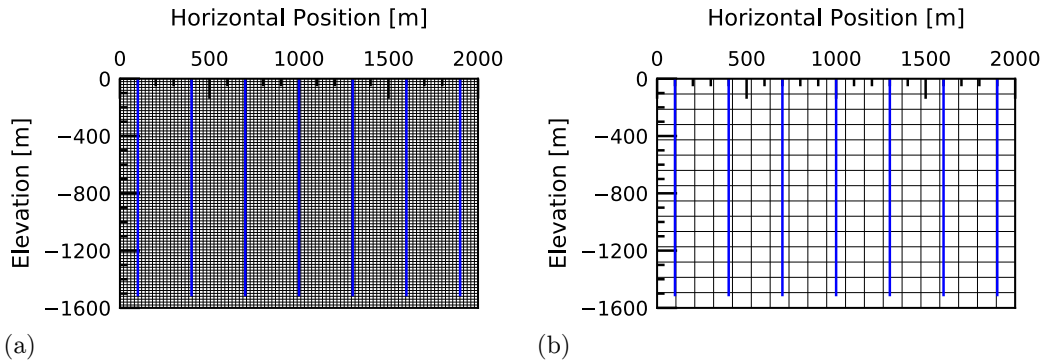


Figure A.1. Computational grids used to simulate the geothermal system. The fine model geometry (a) consisted of a square grid of $81 \times 100 = 8100$ blocks (including one layer of atmospheric blocks), and the coarse model (b) consisted of a grid of $17 \times 20 = 340$ blocks (again including one layer of atmospheric blocks). Observation wells are shown as blue vertical lines.

B Geometric View of BAE

In Figure B.1 below we give a geometric picture of both the standard prior-based and our posterior-based composite (enhanced) error model approach. In both cases we essentially aim to conservatively cover the deterministic functional relationship $p(\boldsymbol{\varepsilon}|\mathbf{k})$, or the associated degenerate joint distribution $p(\boldsymbol{\varepsilon}|\mathbf{k})p(\mathbf{k})$, by a probability distribution based on marginal distributions. In the posterior case, however, we restrict attention to estimating the error by sampling over the support of the naive posterior. As can be seen in the figure, the accuracy of this procedure depends on, for example, how well the naive posterior approximates the true posterior. Alternatively, if the error is approximately independent of the parameter, hence giving a horizontal line for $p(\boldsymbol{\varepsilon}|\mathbf{k})$, then both the prior and posterior error distributions would give the same delta distribution for the error, regardless of how well the naive posterior approximates the true posterior. Thus, intuitively, the procedure would be expected to be most reasonable when a) the naive posterior approximates the true posterior reasonably well and/or b) when the model error does not depend strongly on the parameter. This latter condition is already a condition for the usual enhanced/composite error model approach to providing a reason-

able approximation, and so switching to the posterior composite error model is at least consistent with this assumption.

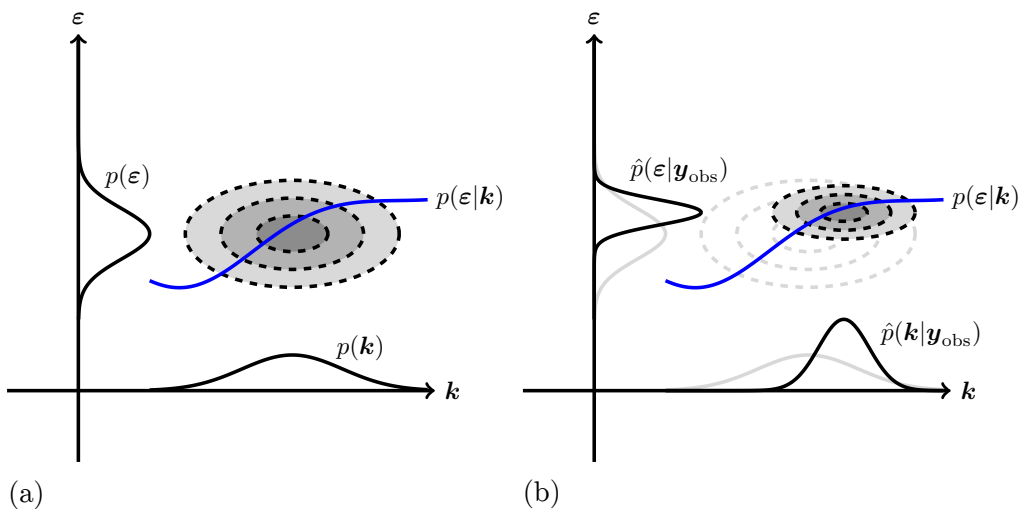


Figure B.1. Geometric interpretation of the enhanced/composite Bayesian model approximation error approach in both (a) the usual prior-based case and (b) our posterior-based approach. In both cases we essentially aim to conservatively cover the deterministic functional relationship $p(\varepsilon|\mathbf{k})$, or the associated degenerate joint distribution $p(\varepsilon|\mathbf{k})p(\mathbf{k})$, by a probability distribution based on marginal distributions. In the posterior case, however, we restrict attention to estimating the error by sampling over the support of the naive posterior.

C Corner Plots



Figure C.1. Corner plots illustrating both marginal and bivariate distributions for rock permeabilities (log scale) under the naive, uncorrected model. A number of the true parameters lie outside the bulk of the support of the posterior.

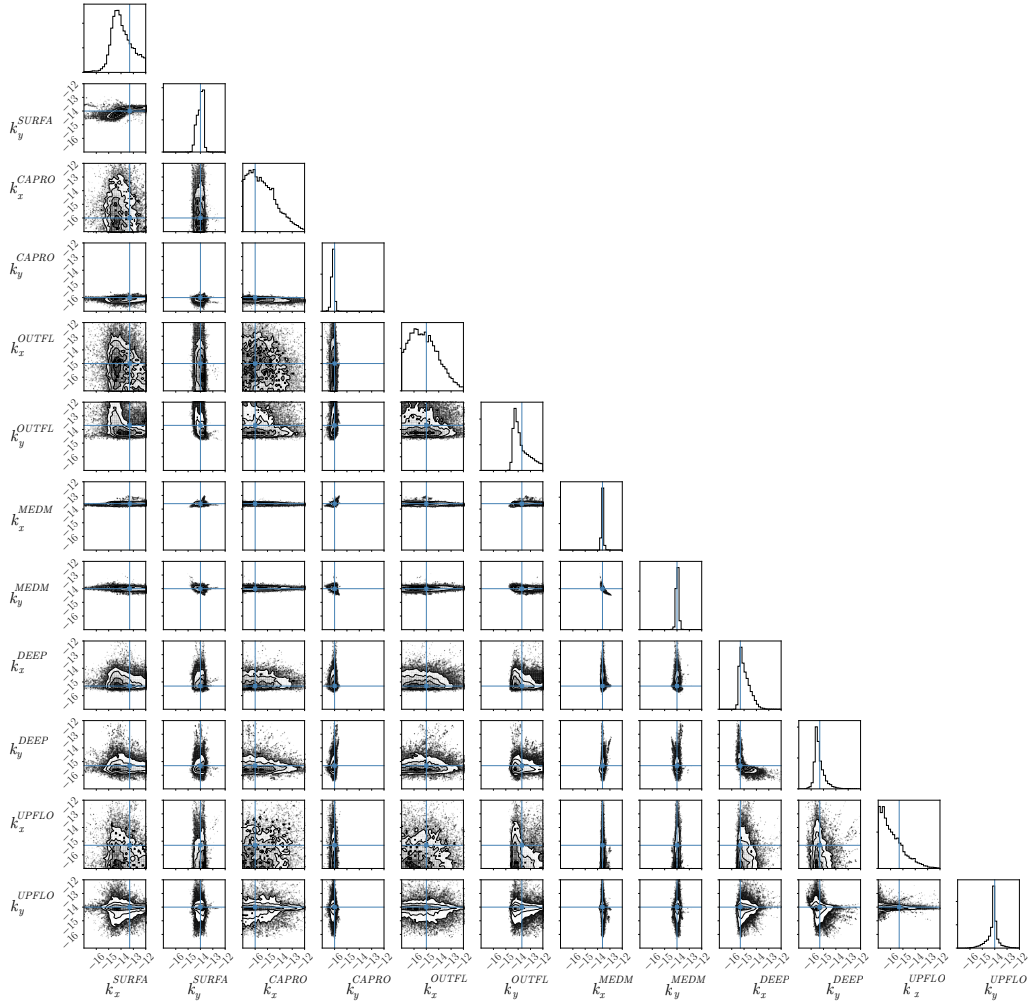


Figure C.2. Corner plots illustrating both marginal and bivariate distributions for rock permeabilities (log scale) under the model-discrepancy-corrected model. All parameters are contained in the bulk of the support of the posterior.

Acknowledgments

The authors appreciate the contribution of the NZ Ministry of Business, Innovation and Employment for funding parts of this work through the grant: C05X1306 Geothermal Supermodels. The authors would also like to thank Jari Kaipio for helpful discussions about Bayesian approximation error methods. Our code is available from <https://github.com/omaclaren/hierarchical-bae-manuscript>.

References

- Aanonsen, S. I. (2005). Efficient history matching using a multiscale technique. In *SPE Reservoir Simulation Symposium*.
- Au, C. and Tam, J. (1999). Transforming variables using the dirac generalized function. *Am. Stat.*, 53(3):270–272.
- Berliner, L. M. (1996). Hierarchical Bayesian time series models. In *Maximum entropy and Bayesian methods*, pages 15–22. Springer.
- Berliner, L. M. (2003). Physical-statistical modeling in geophysics. *Journal of Geophysical Research: Atmospheres*, 108(D24).
- Berliner, L. M. (2012). Statistical approaches to combining models and observations. *SIAM News*, 45(7).
- Bjarkason, E. K., Maclaren, O. J., O’Sullivan, J. P., and O’Sullivan, M. J. (2018). Randomized truncated SVD Levenberg-Marquardt approach to geothermal natural state and history matching. *Water Resources Research*, 54(3):2376–2404.
- Bjarkason, E. K., O’Sullivan, M. J., O’Sullivan, J. P., and Yeh, A. (2016). Accelerating calibration of natural state geothermal models. In *41st Workshop on Geothermal Reservoir Engineering*, Stanford University, Stanford California.
- Burnell, J., Clearwater, E., Croucher, A., Kissling, W., O’Sullivan, J., O’Sullivan, M., and Yeh, A. (2012). Future directions in geothermal modelling. In *Proceedings 34th New Zealand Geothermal Workshop*.
- Carpenter, B., Gelman, A., Hoffman, M. D., Lee, D., Goodrich, B., Betancourt, M., Brubaker, M., Guo, J., Li, P., and Riddell, A. (2017). Stan: A probabilistic programming language. *Journal of statistical software*, 76(1).
- Croucher, A. (2011). PyTOUGH: a Python scripting library for automating TOUGH2 simulations. In *The New Zealand Geothermal Workshop*, volume 21.
- Croucher, A., O’Sullivan, J., Yeh, A., and O’Sullivan, M. (2018). Benchmarking and experiments with Waiwera, a new geothermal simulator.
- Cui, T., Fox, C., and O’Sullivan, M. (2011). Bayesian calibration of a large-scale geothermal reservoir model by a new adaptive delayed acceptance metropolis hasting’s algorithm. *Water Resources Research*, 47(10).
- Doherty, J. (2015). PEST, model-independent parameter estimation: user manual, 5th edn.(and addendum to the PEST manual). *Watermark, Brisbane*,

- Australia. Available at www.pesthomepage.org.*
- Doherty, J. and Christensen, S. (2011). Use of paired simple and complex models to reduce predictive bias and quantify uncertainty. *Water Resour. Res.*, 47(12):154.
- Evans, M. (2015). *Measuring Statistical Evidence Using Relative Belief*. Chapman & Hall/CRC Monographs on Statistics & Applied Probability. CRC Press.
- Evans, S. N. and Stark, P. B. (2002). Inverse problems as statistics. *Inverse Problems*, 18(4):R55.
- Finsterle, S. (2000). iTOUGH2 user’s guide. Lawrence Berkeley National Laboratory. *University of California, Berkeley, CA*, 130.
- Foreman-Mackey, D. (2016). corner.py: Scatterplot matrices in Python. *The Journal of Open Source Software*, 24.
- Foreman-Mackey, D., Hogg, D. W., Lang, D., and Goodman, J. (2013). emcee: The mcmc hammer. *Publications of the Astronomical Society of the Pacific*, 125(925):306.
- Goodman, J. and Weare, J. (2010). Ensemble samplers with affine invariance. *Communications in Applied Mathematics and Computational Science*, 5(1):65–80.
- Huijser, D., Goodman, J., and Brewer, B. J. (2015). Properties of the affine invariant ensemble sampler in high dimensions.
- Huttunen, J. and Kaipio, J. (2009). Model reduction in state identification problems with an application to determination of thermal parameters. *Applied Numerical Mathematics*.
- Kaipio, J. and Kolehmainen, V. (2013). Approximate marginalization over modeling errors and uncertainties in inverse problems. In Damien, P., Dellaportas, P., Polson, N. G., and Stephens, D. A., editors, *Bayesian Theory and Applications*, pages 644–672. Oxford University Press.
- Kaipio, J. and Somersalo, E. (2005). *Statistical and Computational Inverse Problems*. Springer.
- Kaipio, J. and Somersalo, E. (2007). Statistical inverse problems: Discretization, model reduction and inverse crimes. *Journal of Computational and Applied Mathematics*, 198(2):493–504.
- Kennedy, M. C. and O’Hagan, A. (2000). Predicting the output from a complex computer code when fast approximations are available. *Biometrika*.

- Khuri, A. I. (2004). Applications of dirac’s delta function in statistics. *Internat. J. Math. Ed. Sci. Tech.*, 35(2):185–195.
- Kolehmainen, V., Schweiger, M., Nissilä, I., Tarvainen, T., Arridge, S. R., and Kaipio, J. P. (2009). Approximation errors and model reduction in three-dimensional diffuse optical tomography. *J. Opt. Soc. Am. A*, 26(10):2257–2268.
- Lehikoinen, A., Huttunen, J. M. J., Finsterle, S., Kowalsky, M. B., and Kaipio, J. P. (2010). Dynamic inversion for hydrological process monitoring with electrical resistance tomography under model uncertainties. *Water Resources Research*, 46(4).
- Lødøen, O. P. and Omre, H. (2008). Scale-corrected ensemble kalman filtering applied to production-history conditioning in reservoir evaluation. *SPE journal*, 13(02):177–194.
- Maclaren, O. J., Bjarkason, E., O’Sullivan, J., and O’Sullivan, M. J. (2016). Inverse modelling of geothermal reservoirs - A hierarchical Bayesian approach. In *Proceedings 38th New Zealand Geothermal Workshop*, Auckland, New Zealand.
- Mannington, W., O’Sullivan, M., and Bullivant, D. (2004). Computer modelling of the Wairakei–Tauhara geothermal system, new zealand. *Geothermics*, 33(4):401–419.
- Nicholson, R., Petra, N., and Kaipio, J. P. (2018). Estimation of the Robin coefficient field in a Poisson problem with uncertain conductivity field. *Inverse Problems*, 34(11):115005.
- Nissinen, A., Heikkinen, L. M., and Kaipio, J. P. (2008). The Bayesian approximation error approach for electrical impedance tomography - experimental results. *Measurement Science and Technology*, 19(1):015501.
- O’Sullivan, J., Dempsey, D., Croucher, A., Yeh, A., and O’Sullivan, M. (2013). Controlling complex geothermal simulations using PyTOUGH. In *Proceedings*. pangea.stanford.edu.
- O’Sullivan, M. J. and O’Sullivan, J. P. (2016). Reservoir modeling and simulation for geothermal resource characterization and evaluation. In DiPippo, R., editor, *Geothermal Power Generation*, pages 165–199. Woodhead Publishing.
- O’Sullivan, M. J., Pruess, K., and Lippmann, M. J. (2001). State of the art of geothermal reservoir simulation. *Geothermics*, 30(4):395–429.

- O’Sullivan, M. J., Yeh, A., and Mannington, W. I. (2009). A history of numerical modelling of the Wairakei geothermal field. *Geothermics*, 38(1):155–168.
- Patil, A., Huard, D., and Fonnesbeck, C. J. (2010). PyMC: Bayesian stochastic modelling in Python. *Journal of statistical software*, 35(4):1.
- Pruess, K., Oldenburg, C. M., and Moridis, G. J. (1999). TOUGH2 user’s guide version 2.
- Pulkkinen, A., Cox, B. T., Arridge, S. R., Goh, H., Kaipio, J. P., and Tarvainen, T. (2016). Direct estimation of optical parameters from photoacoustic time series in quantitative photoacoustic tomography. *IEEE Transactions on Medical Imaging*, 35(11):2497–2508.
- Stuart, A. M. (2010). Inverse problems: A Bayesian perspective. *Acta Numerica*, 19:451–559.
- Tarantola, A. (2004). *Inverse Problem Theory and Methods for Model Parameter Estimation*. Society for Industrial and Applied Mathematics.
- Tarvainen, T., Kolehmainen, V., Pulkkinen, A., Vauhkonen, M., Schweiger, M., Arridge, S. R., and Kaipio, J. P. (2010). An approximation error approach for compensating for modelling errors between the radiative transfer equation and the diffusion approximation in diffuse optical tomography. *Inverse Problems*, 26(1):015005.
- Trehan, S. and Durlflosky, L. J. (2018). Machine-learning-based modeling of coarse-scale error, with application to uncertainty quantification. *Computational Geosciences*, 22(4):1093–1113.
- Varin, C. (2008). On composite marginal likelihoods. *AStA*, 92(1):1.
- Varin, C., Reid, N., and Firth, D. (2011). An overview of composite likelihood methods. *Stat. Sin.*, 21(1):5–42.
- Yeh, A., Croucher, A. E., and O’Sullivan, M. J. (2012). Recent developments in the AUTOUGH2 simulator. *Proc, TOUGH Symposium, Lawrence Berkeley*.